Disproportionation and thermochemical sulfate reduction reactions in S–H$_2$O–CH$_4$ and S–D$_2$O–CH$_4$ systems from 200 to 340 °C at elevated pressures

Shunda Yuan [a,b,c,*], I-Ming Chou [c,d], Robert C. Burruss [e], Xiaolin Wang [f], Jiankang Li [a]

[a] MLR Key Laboratory of Metallogeny and Mineral Assessment, Institute of Mineral Resources, CAGS, Beijing 100037, PR China
[b] State Key Laboratory of Ore Deposit Geochemistry, Institute of Geochemistry, Chinese Academy of Sciences, Guiyang 550002, PR China
[c] U.S. Geological Survey, 954 National Center, Reston, VA 20192, USA
[d] Laboratory for Experimental Study Under Deep-sea Extreme Conditions, Sanya Institute of Deep Sea Science and Engineering, Chinese Academy of Sciences, Sanya 572000, PR China
[e] U.S. Geological Survey, 956 National Center, Reston, VA 20192, USA
[f] State Key Laboratory for Mineral Deposits Research & Institute of Energy Sciences, School of Earth Sciences and Engineering, Nanjing University, Nanjing 210093, PR China

Abstract

Elemental sulfur, as a transient intermediate compound, by-product, or catalyst, plays significant roles in thermochemical sulfate reduction (TSR) reactions. However, the mechanisms of the reactions in S–H$_2$O–hydrocarbons systems are not clear. To improve our understanding of reaction mechanisms, we conducted a series of experiments between 200 and 340 °C for S–H$_2$O–CH$_4$, S–D$_2$O–CH$_4$, and S–CH$_4$–1m ZnBr$_2$ systems in fused silica capillary capsules (FSCCs). After a heating period ranging from 24 to 2160 h (hrs), the quenched samples were analyzed by Raman spectroscopy. Combined with the *in situ* Raman spectra collected at high temperatures and pressures in the S–H$_2$O and S–H$_2$O–CH$_4$ systems, our results showed that (1) the disproportionation of sulfur in the S–H$_2$O–CH$_4$ system occurred at temperatures above 200 °C and produced H$_2$S, SO$_4^{2-}$, and possibly trace amount of HSO$_4^-$; (2) sulfate (and bisulfate), in the presence of sulfur, can be reduced by methane between 250 and 340 °C to produce CO$_2$ and H$_2$S, and these TSR temperatures are much closer to those of the natural system (<200 °C) than those of any previous experiments; (3) the disproportionation and TSR reactions in the S–H$_2$O–CH$_4$ system may take place simultaneously, with TSR being favored at higher temperatures; and, (4) in the system S–D$_2$O–CH$_4$, both TSR and the competitive disproportionation reactions occurred simultaneously at temperatures above 300 °C, but these reactions were very slow at lower temperatures. Our observation of methane reaction at 250 °C in a laboratory time scale suggests that, on a geologic time scale, methane may be destroyed by TSR reactions at temperatures >200 °C that can be reached by deep drilling for hydrocarbon resources.
© 2013 Elsevier Ltd. All rights reserved.

1. INTRODUCTION

The thermochemical sulfate reduction (TSR) reaction is a thermally-driven, abiological reduction of sulfate by hydrocarbons at temperatures probably less than 200 °C in natural systems producing combinations of H$_2$S, CO$_2$, carbonate minerals (e.g., calcite), elemental sulfur, various

---

* Corresponding author at: MLR Key Laboratory of Metallogeny and Mineral Assessment, Institute of Mineral Resources, CAGS, Beijing 100037, PR China.

E-mail address: sdyuan011981@yahoo.com.cn (S. Yuan).

organic sulfur compounds, and water (Krouse et al., 1988; Machel et al., 1995; Worden and Smalley, 1996; Worden et al., 2000; Machel, 2001; Cross et al., 2004). TSR reactions are considered to be important for the origin of high H_2S concentrations in petroleum reservoirs and for the deposition of metal sulfides in ore deposits (Barton, 1967; Orr, 1974, 1977; Anderson, 1975, 1983, 1991, 2008; Powell and Macqueen, 1984; Anderson and Garven, 1987; Machel, 1987; Worden et al., 1995; Worden and Smalley, 1996; Sangster et al., 1998; Sun and Puttmann, 2000; Alonso-Azcárate et al., 2001; Cai et al., 2003, 2005; Garven et al., 2003; Anderson and Thom, 2008; Basuki et al., 2008; Thom and Anderson, 2008). Hydrogen sulfide produced by TSR in oil and gas is considered to be an undesirable component of natural gas, because it not only dilutes the proportion of hydrocarbon gas, but it is also highly toxic and corrosive, resulting in operational, environmental, and treatment-related problems (Worden and Smalley, 1996; Cross et al., 2004; Mougin et al., 2007). Therefore, better understanding of the mechanisms and kinetics of TSR has become a prerequisite to enhance our ability to predict H_2S concentrations in gas reservoirs in sedimentary basins and to minimize its unwanted effects (Worden and Smalley, 1996; Pan et al., 2006). Even though geological observations and experimental studies of TSR have been extensive in the past five decades (e.g., Sassen and Moore, 1988; Kiyosu and Krouse, 1993; Cross et al., 2004; Ding et al., 2008; Zhang et al., 2008a,b; Watanabe et al., 2009), only a limited number of experimental investigations were performed to evaluate the reduction of sulfate by methane. Moreover, most of these experiments (Yue et al., 2005, 2006; Ding et al., 2008; Chou et al., 2008b) were conducted at temperatures much higher than those in the natural geologic settings (Zhang et al., 2008b). Also, it is still controversial whether methane, the predominant component of natural gases, actually participates in natural TSR reactions (Barton, 1967; Krouse et al., 1988; Rhodes, 1994; Machel et al., 1995; Worden and Smalley, 1996, 2004; Worden et al., 2000; Machel, 2001; Cai et al., 2004; Pan et al., 2006; Hao et al., 2008; Zhang et al., 2008b).

There are also uncertainties about the role of elemental sulfur in TSR reactions. Sulfur commonly occurs in sour gas reservoirs in sulfate-bearing carbonate reservoir rocks and it is not clear whether sulfur is a transient intermediate compound or a by-product of TSR reactions (Machel, 1987, 1989; Krouse et al., 1988; Heydari and Moore, 1989; Kiyosu and Krouse, 1993; Machel et al., 1995; Worden and Smalley, 1996; Heydari, 1997; Alonso-Azcárate et al., 2001; Seewald, 2003). Previous geologic studies indicated that elemental sulfur could be produced by reduction of sulfate by C_{2+} hydrocarbons (Orr, 1974; Worden and Smalley, 1996; Worden et al., 1996), and then react with methane and other hydrocarbons to produce H_2S and CO_2 (Orr, 1974; Machel et al., 1995; Worden and Smalley, 1996; Heydari, 1997). A number of experimental studies indicated that elemental sulfur plays a significant role in TSR reactions (Toland, 1960; Douglas and Mair, 1965; Kiyosu and Krouse, 1993; Goldhaber and Orr, 1995), but the role of sulfur in TSR reactions in the $S–H_2O–CH_4$ system is not known.

We have begun to investigate the mechanisms of TSR reactions using an experimental method in which fused silica capillary capsules (FSCCs) are used as the reaction vessels for investigations of hydrothermal reactions (Shang et al., 2008; Chou et al., 2008b; Yuan et al., 2009). The combination of FSCC and Raman spectroscopy has provided great opportunity for *in situ* analysis under reaction temperature–pressure conditions. At the beginning of our experiments, we carried out many short-duration (up to 46 min) *in situ* experiments at temperatures up to 450 °C for the systems containing S, H_2O, and CH_4 (Yuan et al., 2009). However, due to the slow reaction rate of TSR in these systems, the products of TSR reactions are difficult to detect in these short-duration *in situ* experiments. Nevertheless, these preliminary results provided guidance for our long-duration experiments, in which the products were analyzed after quenching. Results of both types of experiments will be presented below. The objectives of this study are to (1) better understand the processes of the reactions in the $S–H_2O–CH_4$ system and evaluate reaction pathways, (2) evaluate the potential for TSR reactions in the $S–H_2O–CH_4$ system at relatively low temperatures, and (3) evaluate the extent of these TSR reactions.

2. EXPERIMENTAL AND ANALYTICAL METHODS

2.1. Experimental methods

Fused silica capillary capsules (FSCCs), prepared from capillaries purchased from Polymicro Technologies, LLC (http://polymicro.com), were used as the reactors in this study. The sample loading procedures, similar to those of Chou et al. (2008a) and Shang et al. (2009), include the following steps: (1) the sample capsules were prepared by first loading the elemental sulfur (99.9999%, Atomergic Chemetals Corp.) from one end of a fused silica tube (0.3 mm OD, 0.1 mm ID, ~6 cm long), and sealing this end in a hydrogen flame; (2) for samples containing D_2O, the silica tube loaded with elemental sulfur was dried at 50 °C for 12 h to remove H_2O possibly incorporated during loading sulfur; (3) deionized water, 1m $ZnBr_2$ solution, or D_2O (99.96 atom% D, Sigma–Aldrich Co.) was loaded from the open end of the tube and centrifuged to the closed end; and (4) the open end of the tube was connected to a vacuum line, and after air in the sample tube was evacuated, methane (99.99%, Air Products, Inc. Lot No. 122701-2) was loaded cryogenically by immersing the sealed end of the tube in liquid nitrogen at about 0.1–0.2 MPa methane pressure in the vacuum line for a few minutes, and then sealing the open end of the tube with a hydrogen flame while the enclosed end was still frozen in liquid nitrogen under vacuum (Fig. 1).

For short duration experiments, capsules containing S–H_2O and S–H_2O–CH_4 were heated in a USGS-type heating stage from room temperature to 410 °C for up to 46 min. Raman spectra were collected *in situ* at high temperature to look for evidence of rapid reactions in these systems. These experiments provided critical evidence for the limited extent of back reactions during quenching of long-term experiments in these systems.
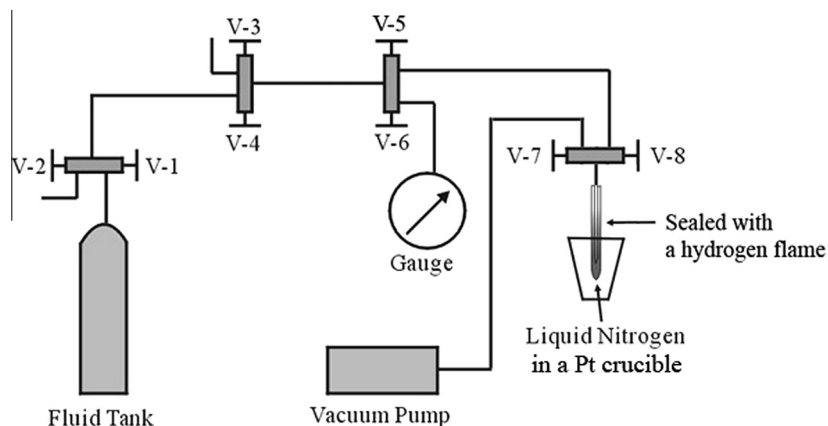
Fig. 1. A schematic diagram of the sample loading system. V-1 to V-8 are three-way/two-stem combination taper-seal valves from High Pressure Equipment Co. (Cat. No. 15-15AF1) (after Chou et al., 2008a,b).

For the long duration experiments, capsules were heated in cold-sealed pressure vessels (CSPVs) at one atmosphere external pressure, and sample temperatures (accurate to ± 3 °C) were monitored by K-type thermocouples with a digital meter. Raman spectra were collected from the quenched FSCCs at room temperature.

2.2. Raman analysis

Raman spectra were acquired with a JY/Horiba Lab-Ram HR Raman system, using 532.06 nm (frequency doubled Nd:YAG) laser excitation, a $40 \times$ Olympus objective with 0.25 numerical aperture, and a 600 grooves/mm grating with a spectral resolution of about 2 cm^{-1}. An approximately 20 mW laser light was focused on a central level of the horizontal tube during the measurement. Raman spectra were collected from 50 to 4200 cm^{-1} for various lengths of time with one to five accumulations per spectrum.

The emission line of a helium–neon (He–Ne) laser at 632.817 nm was collected simultaneously with the Raman spectra. Its peak position at 2992.52 cm^{-1} relative to the 532.06 nm line of the Nd:YAG laser was used as a calibration reference, such that the real peak positions (v_{real}) of the reactants and products can be derived from the measured peak positions of the sample (v_{measured}) and the He–Ne laser light (v_{red}) by the following relationship (Lu et al., 2007):

$$v_{\text{real}}(\text{cm}^{-1}) = 2992.52 + v_{\text{measured}} - v_{\text{red}} \qquad (1)$$

Based on the Raman shifts of CH_4 in the starting vapor phase, the initial sample pressure was calculated by using the following equation (Lu et al., 2007):

$$P(\text{MPa}) = -0.0148 \times D^5 - 0.1791 \times D^4 - 0.8479$$
$$\times D^3 - 1.765 \times D^2 - 5.876 \times D \qquad (2)$$

where D (in cm^{-1}) $= v_p - v_0$, v_p is the CH_4 peak position obtained from the vapor phase in a FSCC sample at room temperature, and v_0 is CH_4 peak position near zero pressure ($\sim 2918 \text{ cm}^{-1}$), obtained from a reference FSCC prepared in our laboratory. During heating, the sample pressure increases, but was difficult to estimate due to unknown thermal expansion of the FSCC under relatively high internal pressure.

2.3. Experiment design

Experiments on the $S–H_2O–CH_4$ and $S–H_2O$ were conducted to test the roles of various reaction mechanisms involved in TSR reaction that have been proposed in previous publications. The long and short duration experiments provide qualitative evidence for the rates of reaction. Experiments with 1m $ZnBr_2$ were conducted to test for reaction reversals involving H_2S by removing H_2S as quickly as it formed as ZnS precipitates. We also conducted experiments with D_2O to examine the possible role of water as a source for hydrogen during the formation of H_2S.

Analytical measurements were made by Raman spectroscopy to allow monitoring of reaction progress at progressively higher temperatures in the same sample without opening the sample capsule. This prevented any possible oxidation of reaction intermediates by exposure to air. Although other analytical methods have much lower detection limits, Raman spectroscopy is the only method that allows non-destructive observation of changes in reactant and product concentrations *in situ* at elevated temperature and pressure.

3. RESULTS

The experimental conditions and results are summarized in Table 1. Annotated spectra are shown in Figs. 2–11. Detailed results for each system are as follows:

3.1. The $S–H_2O–CH_4$ system

The Raman spectra of long duration experiments collected from the aqueous and vapor phases of the samples containing $S–H_2O–CH_4$ quenched from 200, 250, and 340 °C are shown in Figs. 2 and 3, respectively. These figures show that the Raman signals of SO_4^{2-} ($\sim 980 \text{ cm}^{-1}$) in the aqueous phase and H_2S ($\sim 2606 \text{ cm}^{-1}$) in the vapor phase were detected in the quenched sample that reacted at 200 °C for 24 h. In the aqueous phase of the 200 °C sample (Fig. 3), there is a shoulder at 1050 cm^{-1} on a broad band for silica glass that suggests HSO_4^- is possibly present at this temperature. When the same capsule was further

Table 1
Experimental conditions and products detected by Raman spectroscopy.

Starting material	Starting condition[a]		T (°C)	Duration (h)	Products
	Raman peak position (cm^{-1}) for CH$_4$ (ν_1)	Pressure (MPa)[b]			
S–CH$_4$–H$_2$O	2914.22	17.64	200	24	SO$_4^{2-}$, H$_2$S
			250	24	SO$_4^{2-}$, HSO$_4^-$, H$_2$S, CO$_2$
			340	96	H$_2$S, CO$_2$
S–CH$_4$–1m ZnBr$_2$	2915.68	10.49	250	40	SO$_4^{2-}$, HSO$_4^-$, CO$_2$
			300	40	SO$_4^{2-}$, CO$_2$
S–CH$_4$–D$_2$O	2914.37	16.86	250	40	SO$_4^{2-}$, DSO$_4^-$, CO$_2$
			300	40	SO$_4^{2-}$, CO$_2$, D$_2$S
			300	2160	CO$_2$, D$_2$S, H$_2$S

[a] The lengths of all fused silica capillary capsules are about 10 mm, and the initial ratios between vapor and aqueous phase are about 1:2.
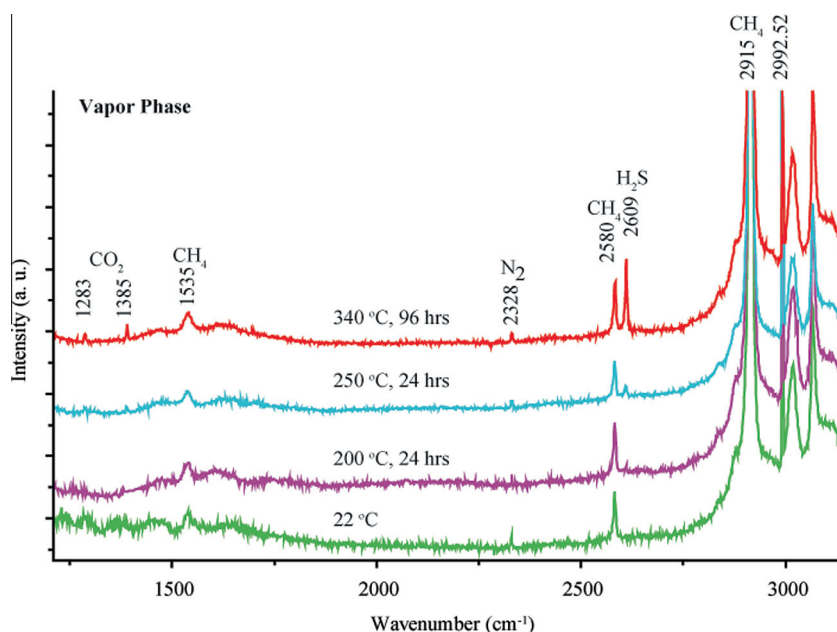[b] Calculated form Eq (2).

Fig. 2. Raman spectra collected from the vapor phase of a quenched FSCC containing S, H$_2$O, and CH$_4$, after heating at 200, 250, and 340 °C for 24 to 96 h at each temperature. Also shown is the Raman spectrum of the initial sample at 22 °C. The peak at 2992.52 cm^{-1} is a calibration signal from a He–Ne laser of 632.817 nm wavelength. The peak at 2328 cm^{-1} resulted from N$_2$ in air.

heated at 250 °C for 24 h, the spectrum for the aqueous phase (Fig. 3) showed reduction of SO$_4^{2-}$ and HSO$_4^-$ Raman band intensity as well as the presence of H$_2$S. Also, the Raman spectrum of the quenched vapor phase (Fig. 2) showed the presence of CO$_2$ ($\sim$1283 and $\sim$1385 cm^{-1}) and H$_2$S. When the same sample capsule was further heated at 340 °C for 96 h, the Raman band intensities of CO$_2$ and H$_2$S in the quenched vapor phase increased significantly and the SO$_4^{2-}$ and HSO$_4^-$ bands in the quenched aqueous phase disappeared.

3.2. In situ experimental results of the systems S–H$_2$O and S–H$_2$O–CH$_4$

Short duration in situ Raman spectra for S–H$_2$O system were recorded for the aqueous phase and the homogenized phase (Fig. 4) and the vapor phase and the homogenized phase (Fig. 5). The time spans at the specified temperatures were shown in Figs. 4 and 5. In the aqueous phase the Raman band of H$_2$S was observed after 18 min at temperatures of 250 °C and higher. Soon after L–V homogenization at 369 °C, weak Raman signals of HSO$_4^-$ and SO$_2$ can be detected. The band for SO$_2$ increases in intensity on further heating, but the weak band for HSO$_4^-$ disappears. During cooling, the Raman signal for SO$_2$ became weaker, and only weak Raman signals of SO$_4^{2-}$ and H$_2$S can be detected 1 day after cooling to room temperature. In the vapor phase (Fig. 5), the Raman bands of H$_2$S and SO$_2$ can be detected at temperatures above 250 and 320 °C, respectively. During cooling, the reduction of Raman signals of SO$_2$ can be observed, and only weak Raman signals of H$_2$S can be detected 1 day after cooling to room temperature.
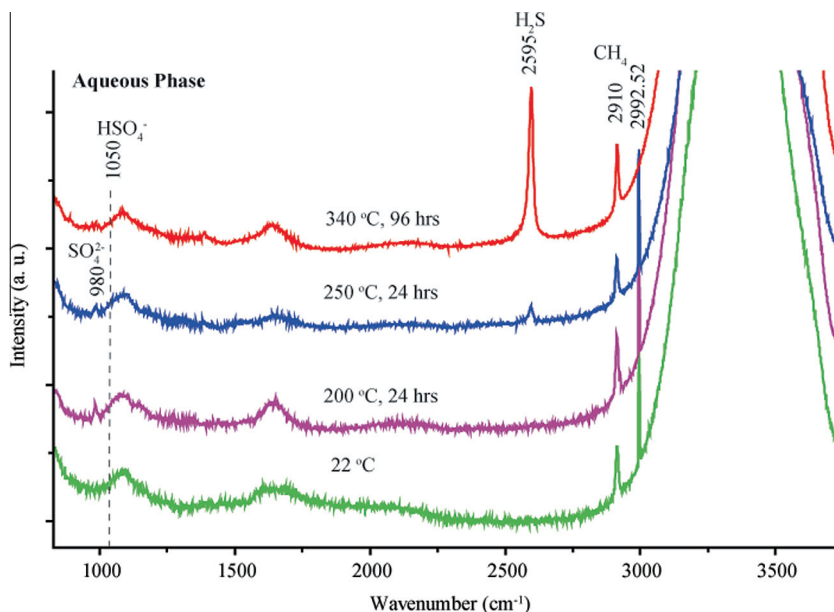
Fig. 3. Raman spectra collected from the aqueous phase of a quenched FSCC containing S, H_2O, and CH_4, after heating at 200, 250, and 340 °C for 24 to 96 h at each temperature. Also shown is the Raman spectrum of the initial sample at 22 °C. The small shoulder at 1050 cm^{-1} for the spectra at 200 °C indicates the presence of HSO_4^- near or below the detection limit. The peak at 2992.52 cm^{-1} is a calibration signal from a He–Ne laser of 632.817 nm.
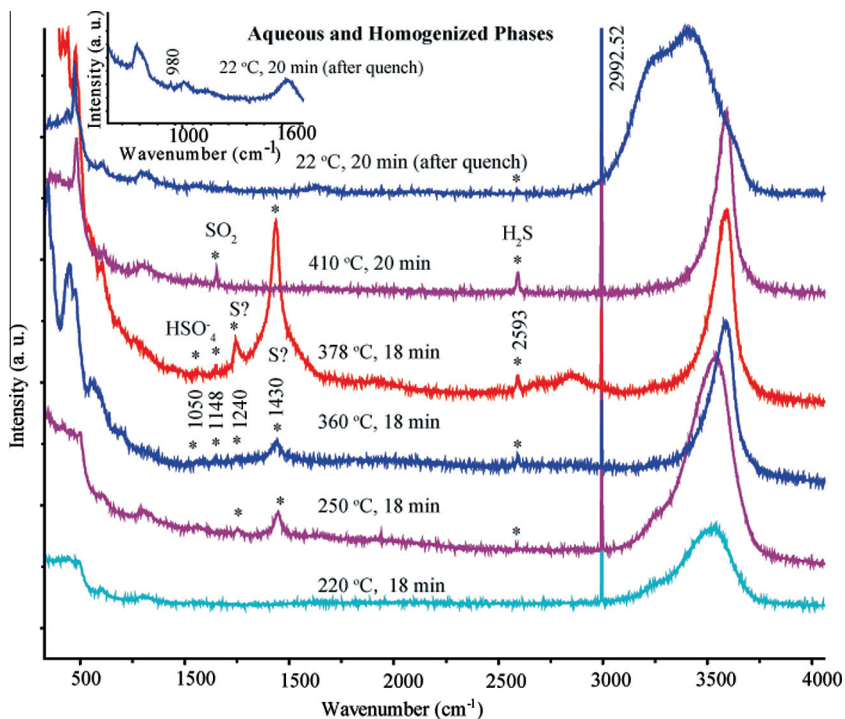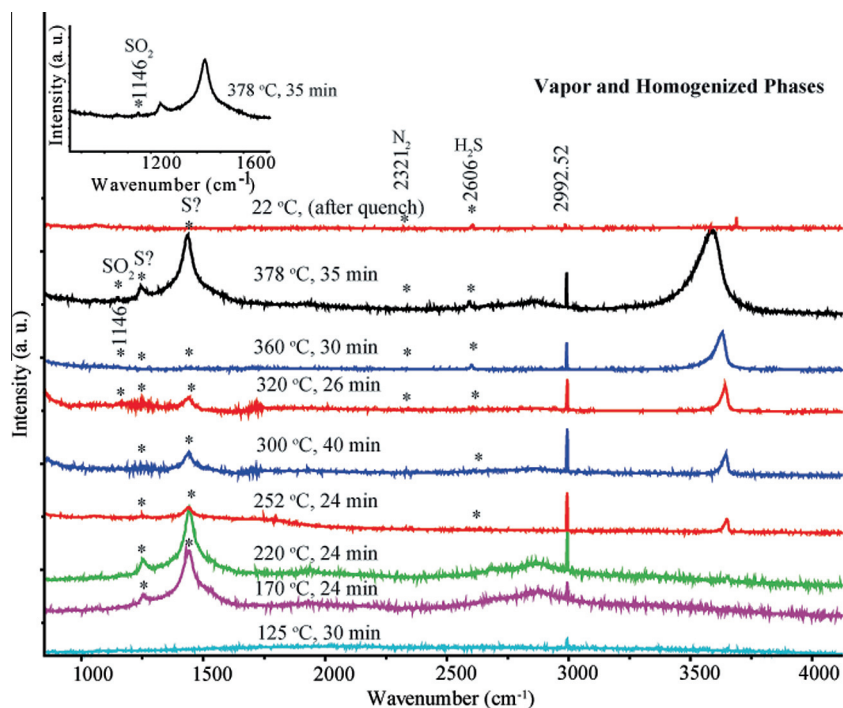

Fig. 4. *In situ* Raman spectra collected from a FSCC containing S and H_2O during heating and cooling in a USGS heating–cooling stage. The spectra shown are for the aqueous phase below the homogenization temperature ($\sim$369 °C) and also for the homogeneous phase above 369 °C. The time spans at the specified temperatures were shown. Note the disproportionation of S to produce H_2S (2593 cm^{-1}), SO_2 (1148 cm^{-1}), and possibly HSO_4^- (1050 cm^{-1}) during heating, and the disappearance of SO_2 after cooling to room temperature. The insert shows the SO_4^{2-} (980 cm^{-1}) signal in the aqueous phase at room temperature. The signals at 1240 and 1430 cm^{-1} were from unknown S-bearing species and the signal at 2992.52 cm^{-1} is calibration signal from a He–Ne laser of 632.817 nm.
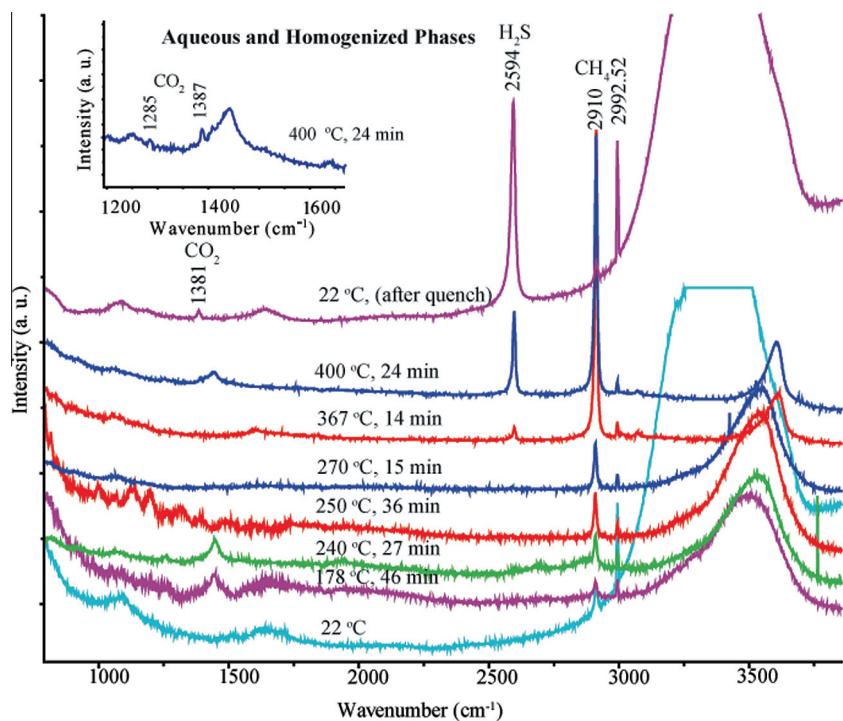
Fig. 5. *In situ* Raman spectra collected from FSCC containing S and H_2O during heating and cooling in a USGS heating–cooling stage. The spectra shown are for the vapor phase below the homogenization temperature ($\sim$369 °C) and also for the homogeneous phase above 369 °C. The time spans at the specified temperatures were shown. The insert shows the SO_2 (1146 cm^{-1}) signal in the homogeneous phase at 378 °C. For other information, see Fig. 4.

Fig. 6. *In situ* Raman spectra collected from a FSCC containing S, H_2O and CH_4 during heating and cooling in a USGS heating–cooling stage. The spectra shown are for the aqueous phase below the homogenization temperature ($\sim$366 °C) and also for the homogeneous phase above 366 °C. The time spans at the specified temperatures were shown. Note the formation of CO_2 and H_2S during heating. The insert shows the CO_2 (1285 and 1387 cm^{-1}) signals in the homogeneous phase at 400 °C. The peak at 2992.52 cm^{-1} is a calibration signal from a He–Ne laser of 632.817 nm.
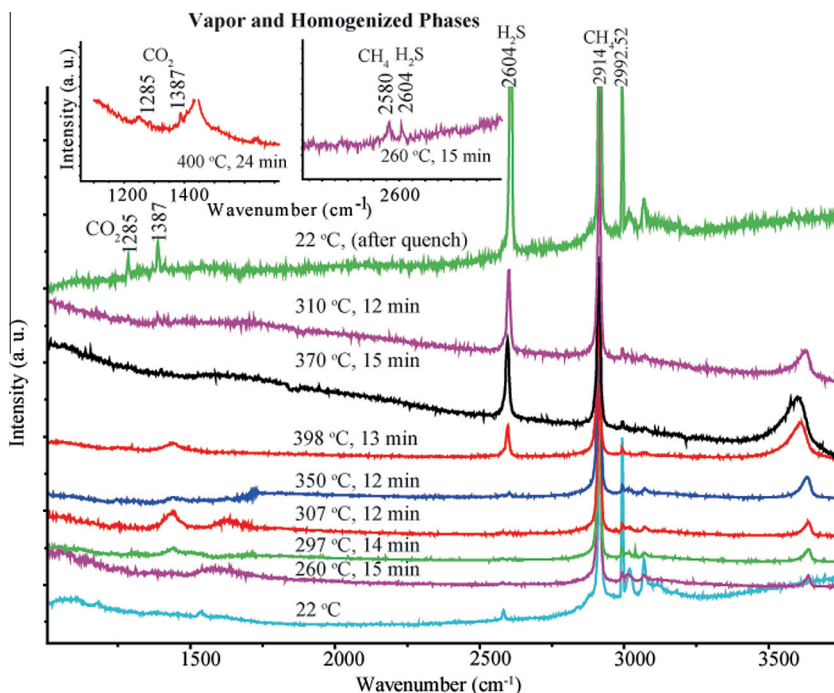
Fig. 7. *In situ* Raman spectra collected from a FSCC containing S, H_2O and CH_4 during heating and cooling in a USGS heating–cooling stage. The spectra shown are for the vapor phase below the homogenization temperature ($\sim$366 °C) and also for the homogeneous phase above 366 °C. The time spans at the specified temperatures were shown. Note the formation of CO_2 and H_2S during heating. The inserts show the H_2S (2604 cm^{-1}) and CH_4 (2580 cm^{-1}) signals in the vapor phase at 260 °C, and the CO_2 (1285 and 1387 cm^{-1}) signals in the homogeneous phase at 400 °C. The peak at 2992.52 cm^{-1} is a calibration signal from a He–Ne laser of 632.817 nm.
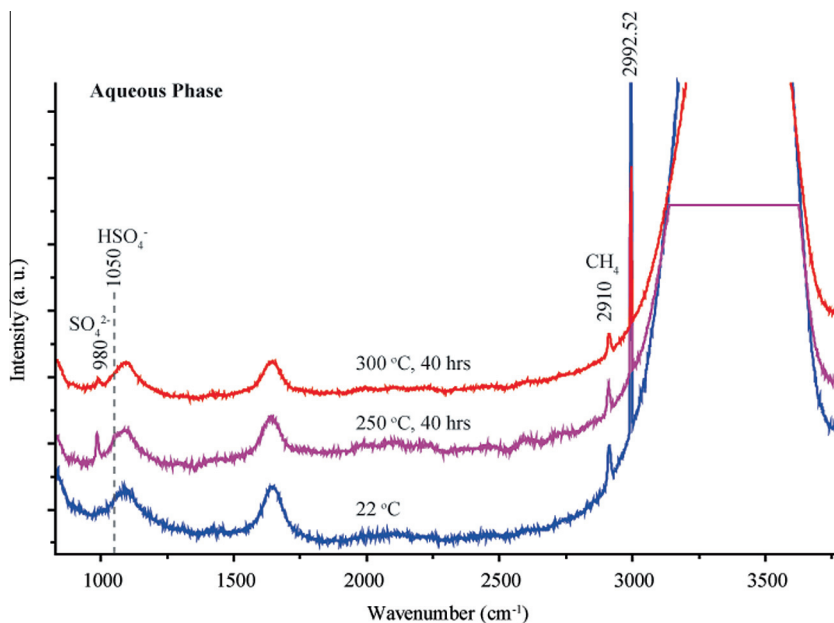

Fig. 8. Raman spectra collected from the aqueous phase of a quenched FSCC containing S–CH_4–1m $ZnBr_2$ after heating at 250 and 300 °C for 40 h at each temperature. The shoulder at 1050 cm^{-1} for the spectrum at 250 °C clearly indicates the presence of HSO_4^- at this temperature, but it disappeared at 300 °C. Also note the reduction of both Raman signals for SO_4^{2-} (980 cm^{-1}) and CH_4 (2910 cm^{-1}). The peak at 2992.52 cm^{-1} is a calibration signal from a He–Ne laser of 632.817 nm.

In situ Raman spectra collected from the aqueous phase (together with the homogenized phase) and the vapor phase (together with the homogenized phase) of the S–H_2O–CH_4 system were shown in Figs. 6 and 7, respectively. In the aqueous phase (Fig. 6), the Raman bands of H_2S can be observed at temperatures above 250 °C, but those of SO_4^{2-} or

HSO_4^- cannot be detected during heating and cooling. After L–V homogenization at 366 °C, the Raman signals of CO_2 can be detected at 400 °C. In the vapor phase (Fig. 7), the Raman bands of H_2S can be detected at temperatures above 260 °C, but that of SO_2 cannot be detected during heating and cooling.
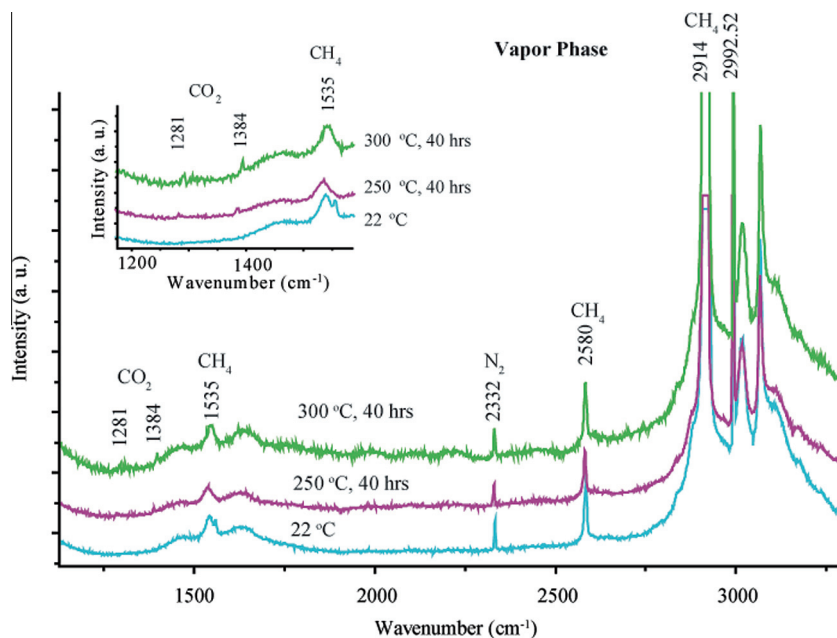

Fig. 9. Raman spectra collected from the vapor phase of a quenched FSCC containing S–CH_4–1m $ZnBr_2$ after heating at 250 and 300 °C for 40 h at each temperature. Also shown is the Raman spectrum of the initial sample at 22 °C. The insert shows the increase of CO_2 signals from 250 to 300 °C. The Raman signal at 2332 cm^{-1} was from N_2 in air. The peak at 2992.52 cm^{-1} is a calibration signal from a He–Ne laser of 632.817 nm.
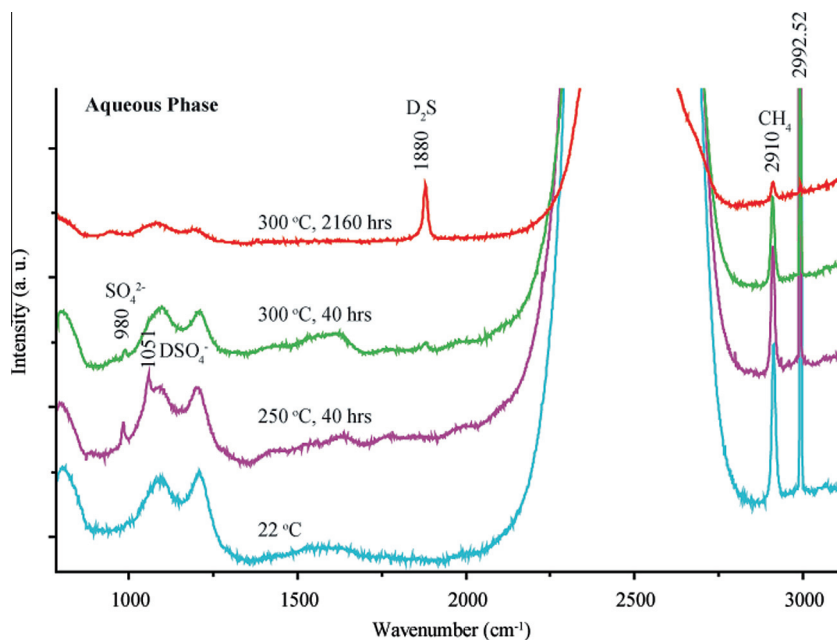

Fig. 10. Raman spectra collected from the aqueous phase of a quenched FSCC containing S–D_2O–CH_4 after heating at 250 and 300 °C for 40 to 2160 h at each temperature. Also shown is the Raman spectrum of the initial sample at 22 °C. Note the presence of DSO_4^- (1051 cm^{-1}) and D_2S (1880 cm^{-1}) at 250 °C. Significant TSR at 300 °C was indicated by the top two spectra showing the consumption of both CH_4 and SO_4^{2-} and the production of D_2S. The peak at 2992.52 cm^{-1} is a calibration signal from a He–Ne laser of 632.817 nm.
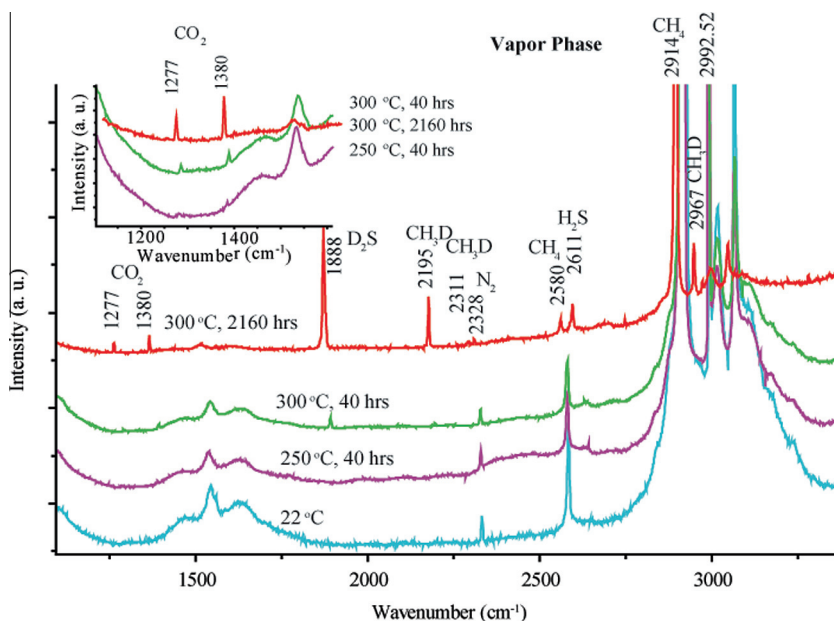
Fig. 11. Raman spectra collected from the vapor phase of a quenched FSCC containing S–D_2O–CH_4 after heating at 250 and 300 °C for 40 to 2160 h at each temperature. Also shown is the Raman spectrum of the initial sample at 22 °C. The insert shows the increase of CO_2 signals from 250 to 300 °C. The peak at 2992.52 cm^{-1} is a calibration signal from a He–Ne laser of 632.817 nm.

3.3. The S–1m $ZnBr_2$–CH_4 system

Results of experiments for S–1m $ZnBr_2$–CH_4 system are shown in Figs. 8 and 9. Raman signals for SO_4^{2-} and CO_2 can be detected, respectively, in the aqueous (Fig. 8) and vapor (Fig. 9) phases quenched from 250 and 300 °C. Moreover, the intensity of SO_4^{2-} and HSO_4^- (1050 cm^{-1}) signals decreased significantly from 250 to 300 °C, and the intensity of CO_2 signal increased from 250 to 300 °C. No significant amount of H_2S was detected due to the formation of dark ZnS precipitates.

### 3.4. The S–D_2O–CH_4 system

Results of the experiments for S–D_2O–CH_4 system at 250 and 300 °C are presented in Figs. 10 and 11, showing that Raman signals can be detected for SO_4^{2-} and DSO_4^- in the aqueous phase and also weak signals for CO_2 in the vapor phase, but neither H_2S nor D_2S Raman signals were detected in the sample quenched from 250 °C. After heating the same capsule at 300 °C for 40 h, Raman spectra showed the presence of D_2S in the quenched sample but not H_2S. When the same capsule was further heated at the same temperature (300 °C) for another 2160 h (90 days), H_2S can be clearly detected with a significant increase of D_2S (Figs. 10 and 11). Finally, we note that CH_3D can be detected in the vapor phase after 90 days of reaction (Fig. 11).

4. DISCUSSION

4.1. Evidence of reactions and mechanisms

The experimental results show that the Raman signals of SO_4^{2-} (~980 cm^{-1}), HSO_4^- (1050 cm^{-1}), and H_2S

(~2606 cm^{-1}) were detected in the quenched S–H_2O–CH_4 sample that reacted at 200 °C for 24 h (Figs. 2 and 3). These products are the result of the disproportionation reaction of sulfur, similar to the hydrolysis reaction of native sulfur described by Toland (1960) and Robinson (1973):

$$4S + 4H_2O \rightarrow SO_4^{2-} + 3H_2S + 2H^+. \quad (3)$$
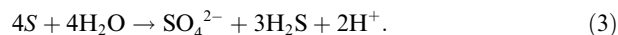
However, the Raman signals of CO_2 were not detected in this capsule, indicating no or limited TSR reaction in this system at 200 °C in 24 h. When the same capsule was further heated at 250 °C for 24 h, the Raman signals collected from the quenched sample showed the presence of CO_2 (~1283 and ~1385 cm^{-1}) and H_2S in the vapor phase (Fig. 2). The reduction of SO_4^{2-} Raman band intensity in the aqueous phase (Fig. 3) as well as the presence of H_2S, indicate the occurrence of TSR:

$$SO_4^{2-} + 2H^+ + CH_4 \rightarrow CO_2 + H_2S + 2H_2O. \quad (4)$$
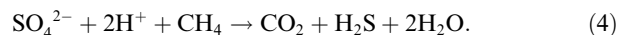
There is limited evidence for the presence of HSO_4^- in the aqueous phase (Fig. 3) at 250 °C. When the same sample capsule was further heated at 340 °C for 96 h, the Raman band intensities of CO_2 and H_2S in the quenched vapor phase increased significantly with the disappearance of SO_4^{2-} and HSO_4^- signals in the quenched aqueous phase, indicating near completion of the TSR reaction.

Previous experiments on TSR reaction showed that the rate of sulfate reduction increases in the presence of hydrogen sulfide (e.g., Zhang et al., 2008a). This appears to be a catalytic effect of H_2S on TSR reaction resulting from the reaction between sulfate and H_2S to produce elemental sulfur (Feely and Kulp, 1957; Orr, 1974, 1977; Dinur et al., 1980; Powell and Macqueen, 1984; Goldhaber and Orr, 1995; Machel et al., 1995; Heydari, 1997; Seewald, 2003; Truche et al., 2009), which then reacted with methane or other hydrocar-

bons and water to produce CO_2 and H_2S (Orr, 1974; Seewald, 2003). Toland (1960) suggested that the catalysis of TSR reaction by low valence sulfur species is more effective at lower pH conditions, although the experiments of Davis et al. (1970) indicate that this reaction is only possible at relatively high temperature conditions. Trudinger et al. (1985) pointed out that the sulfate–sulfide reaction was inhibited by the presence of organic matter. Recently, the experimental studies of Zhang et al. (2008a) suggested that this mechanism may not be important for natural TSR. *In situ* Raman spectroscopy of S–H_2O system at elevated temperature and pressure showed that the intensities of Raman signals of SO_2, and H_2S increased with increasing temperature in the absence of methane, indicating that the disproportionation reactions of sulfur (reactions 3 and 4, above) are enhanced at elevated temperatures (Figs. 4 and 5, Yuan et al., 2009). In addition, *in situ* Raman spectra collected from S–H_2O–CH_4 (from 22 to 400 °C) showed that the Raman signals of SO_4^{2-} and HSO_4^- were not measurable at elevated temperature and pressure (Figs. 6 and 7, Yuan et al., 2009), indicating that the reduction or disappearance of the Raman signals of SO_4^{2-} and HSO_4^- in S–CH_4–H_2O system occurred at elevated temperature rather than during or after quench. Therefore, the extent of the reaction between H_2S and SO_4^{2-} may be very low in S–CH_4–H_2O system under our experimental conditions, and the processes of the catalysis of TSR reaction by low valence sulfur species were probably different from those suggested by previous studies.

Worden and Smalley (1996) and Pan et al. (2006) studied the reaction among sulfur, water, and methane and suggested the following reaction for the consumption of methane and the production of H_2S and CO_2:

$$4S + CH_4 + 2H_2O \rightarrow CO_2 + 4H_2S. \tag{5}$$
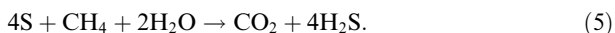
Chen et al. (2009) argued that such reactions between sulfur and hydrocarbons are strictly not a TSR reaction because sulfur rather than sulfate was involved in the reaction. They proposed that reactions in sulfur–hydrocarbon systems are based on catalysis by sulfur radicals. Although Orr (1982) pointed out that the hydrolysis of sulfur may compete with the reaction between sulfate and hydrogen sulfide in the presence of low concentrations of oxidizable organic matter, he did not further discuss the TSR reaction in these systems.

Although reaction (5) does not appear to be a sulfate reduction reaction, this reaction equation can be the result of the sum of two reactions, the disproportionation of sulfur to SO_4^{2-} and H_2S (reaction 3) followed by reduction of sulfate by CH_4 (reaction 4). To test whether this mechanism of TSR in the S–H_2O–CH_4 system will produce CO_2, H_2S, and H_2O, we conducted similar experiments for samples containing S, CH_4, and 1m $ZnBr_2$ solution at 250 and 300 °C. By adding $ZnBr_2$ we effectively excluded the possibility that the loss of SO_4^{2-} was due to reversal of the disproportionation reaction between SO_4^{2-} and H_2S (reaction 3) in these experiments. The $ZnBr_2$ removes H_2S as a ZnS precipitate, as soon as H_2S forms during sulfur disproportionation. The results of these experiments are shown in Figs. 8 and 9. Raman signals for SO_4^{2-} and CO_2 can be detected, respectively, in the aqueous (Fig. 8) and vapor (Fig. 9) phases quenched from 250 and 300 °C. Moreover, the intensity of

SO_4^{2-} signal decreased significantly from 250 to 300 °C, and the intensity of CO_2 signal increased from 250 to 300 °C. No significant amount of H_2S was detected due to the formation of dark ZnS precipitates. This result shows that the loss of SO_4^{2-} from the sample that was quenched from 300 °C was due to the TSR reaction rather than the reaction between SO_4^{2-} and H_2S (i.e., the reverse reaction of the hydrolysis of sulfur). This conclusion is also supported by the corresponding increase in the Raman signal for CO_2 in the quenched FSCC. Therefore, it can be further concluded that the disappearance of SO_4^{2-} and the increase of CO_2 and H_2S for the S–H_2O–CH_4 sample heated to 340 °C, as shown in Figs. 2 and 3, may be ascribed to the TSR reaction between sulfate and methane at elevated temperature rather than the reaction between SO_4^{2-} and H_2S or the reverse reaction of the hydrolysis of sulfur, as shown by reaction (3).

4.2. Evidence that the TSR reaction and competitive disproportionation reactions occurred simultaneously at elevated temperatures

To further test that disproportionation reactions of sulfur are important parts of the TSR process in the S–H_2O–CH_4 system at elevated temperatures, experiments were conducted in the S–D_2O–CH_4 system at 250 and 300 °C. As shown in Figs. 10 and 11, Raman signals can be detected for SO_4^{2-} and DSO_4^- in the aqueous phase and also weak signals for CO_2 in the vapor phase, but neither H_2S nor D_2S Raman signals were detected in the sample quenched from 250 °C, which indicates that both the disproportionation reaction of sulfur and the TSR reaction were very slow at this temperature. After heating the same capsule at 300 °C for 40 h, Raman spectra showed the increase of CO_2 signals and the presence of D_2S in the quenched sample but not H_2S. The presence of D_2S and the increase of CO_2 signals demonstrate the increase of both the disproportionation reaction of sulfur and the TSR reaction. When the same capsule was further heated at the same temperature (300 °C) for another 2160 h (90 days), H_2S can be clearly detected with a significant increase of D_2S and CO_2 (Figs. 10 and 11), indicating the degrees of both TSR and disproportionation reactions increase significantly after long reaction times. Finally, we note that CH_3D can be detected in the vapor phase after 90 days of reaction (Fig. 11). This appears to be a result of isotopic exchange between D_2O or D_2S and CH_4 at elevated temperature.

4.3. Comparison with other laboratory studies

Geologic studies of a number of petroleum reservoirs with evidence of TSR alteration of hydrocarbons indicated that these reactions required temperatures on the order of 140 °C (Worden et al., 1995) for extensive reaction. However, all well documented laboratory simulations of TSR require temperatures >300 °C (see discussion in Zhang et al., 2008b) even in the presence of potential catalysts. None of these studies have indicated that CH_4, the least reactive hydrocarbon, participated in the reactions. The reactions observed in our experiments occurred at temperatures much lower than those reported previously. Furthermore,

we have demonstrated that the disproportionation reaction of sulfur, a key step of TSR in S–H_2O–CH_4 system, occurs in the laboratory at temperatures as low as 200 °C to produce SO_4^{2-} and H_2S, as described by reaction (3). At temperatures above 250 °C, the sulfate and bisulfate are reduced by methane to produce CO_2 and H_2S.

Although our observation of formation of HSO_4^- during some reaction sequences (e.g., Fig 8 in the presence of $ZnBr_2$, and Fig. 10 in the presence of D_2O) could imply that the pH in these experiments was very low, HSO_4^- is only present as a transient trace component in S–H_2O–CH_4 system (Fig. 3). Acid catalysis is known to enhance reaction rates of organic compounds, but there is no evidence that enough bisulfate formed in the S–H_2O–CH_4 system to cause the bisulfate–sulfate ratio to buffer pH to very low values. Furthermore, we have observed in other experiments in the 10 N H_2SO_4–CH_4 system at 300 °C for half a year (Shang et al., unpublished data) that there was no obvious TSR reaction in this acid system. This clearly shows that low pH is not a critical factor in the occurrence of TSR reaction in the systems studied in this work.

A recent study of a high temperature (215 °C) reservoir documented extensive TSR reactions with hydrocarbons including hydrocarbon gases (Mankiewicz et al., 2009). However, the ^{13}C composition of CH_4 showed only a small range of variation suggesting that CH_4 had participated in TSR reaction to only a limited extent. Our observation of methane reaction at 250 °C at laboratory time scales suggests that, at geologic time scales, methane may be destroyed by TSR reactions at temperatures >200 °C that can be reached by deep drilling for hydrocarbon resources.

5. CONCLUSIONS

(1) The disproportionation of sulfur in the S–H_2O–CH_4 system occurred at laboratory temperatures above 200 °C and produced H_2S, SO_4^{2-}, and traces of HSO_4^-.

(2) Sulfate (and bisulfate), in the presence of sulfur, can be reduced by methane between 250 and 340 °C to produce CO_2 and H_2S, and these TSR temperatures are much closer to those of the natural system (<200 °C) than those of any previous experiments.

(3) The disproportionation of sulfur and TSR reactions in the S–H_2O–CH_4 system may take place simultaneously, with TSR reaction being favored at higher temperatures.

REFERENCES

Alonso-Azcárate J., Bottrell S. H. and Tritlla J. (2001) Sulfur redox reactions and formation of native sulfur veins during low grade metamorphism of gypsum evaporates, Cameros basin (NE Spain). *Chem. Geol.* **174**, 389–402.

Anderson G. M. (1975) Precipitation of Mississippi Valley-type ores. *Econ. Geol.* **70**, 937–942.

Anderson G. M. (1983) Some geochemical aspects of sulfide precipitation in carbonate rocks. In: *Internat. Conference on Mississippi Valley type lead-zinc deposits. Proceedings Volume* (eds. G. Kisvarsanyi, S. K. Grant, W. P. Pratt and J. W. Koening). Univ. Missouri-Rolla Press, Rolla, pp. 61–76.

Anderson G. M. (1991) Organic maturation and ore precipitation in Southeast Missouri. *Econ. Geol.* **86**, 909–926.

Anderson G. M. (2008) The mixing hypothesis and the origin of Mississippi Valley-type ore deposits. *Econ. Geol.* **103**, 1683–1690.

Anderson G. M. and Thom J. (2008) The role of thermochemical sulfate reduction in the origin of MVT deposits II. Carbonate–sulfide relationships. *Geofluids* **8**, 27–34.

Anderson G. M. and Garven G. (1987) Sulfate–sulfide–carbonate associations in Mississippi Valley-type lead–zinc deposits. *Econ. Geol.* **82**, 482–488.

Barton, Jr., P. B. (1967) Possible role of organic matter in the precipitation of the Mississippi Valley ores. *Econ. Geol.* **3**, 371–378.

Basuki N. I., Taylor B. E. and Spooner E. T. C. (2008) Sulfur isotope evidence for thermochemical reduction of dissolved sulfate in Mississippi Valley-type zinc–lead mineralization, Bongara area, Northern Peru. *Econ. Geol.* **103**, 783–799.

Cai C. F., Worden R. H., Bottrell S. H., Wang L. S. and Yang C. C. (2003) Thermochemical sulfate reduction and the generation of hydrogen sulfide and thiols (mercaptans) in Triassic carbonate reservoirs from the Sichuan basin, China. *Chem. Geol.* **202**, 39–57.

Cai C., Xie Z., Worden R. H., Hu G., Wang L. and He H. (2004) Methane-dominated thermochemical sulphate reduction in the Triassic Feixianguan Formation East Sichuan Basin, China: towards prediction of fatal H_2S concentrations. *Mar. Pet. Geol.* **21**, 1265–1279.

Cai C. F., Worden R. H., Wolff G. A., Bottrell S. H., Wang D. L. and Li X. (2005) Origin of sulfur rich oils and H_2S in tertiary lacustrine sections of the Jinxian Sag, Bohai Bay Basin, China. *Appl. Geochem.* **20**, 1427–1444.

Chen T. S., He Q., Lu H., Peng P. A. and Liu J. Z. (2009) Thermal simulation experiments of saturated hydrocarbons with calcium sulfate and element sulfur: implications on origin of H_2S. *Sci. China (Ser. D)* **52**, 1550–1558.

Chou I. M., Song Y. C. and Burruss R. C. (2008a) A new method for synthesizing fluid inclusions in fused silica capillaries containing organic and inorganic material. *Geochim. Cosmochim. Acta* **72**, 5217–5231.

Chou I. M., Shang L. B. and Burruss R. C. (2008b) Thermochemical sulfate reduction (TSR) by methane- in situ observation and Raman characterization in fused silica capsules at temperatures up to 450 °C. *Am. Geophys. Union Abstr.*, P43B–1402.

Cross M. M., Manning D. A. C., Bottrell S. H. and Worden R. H. (2004) Thermochemical sulphate reduction (TSR): experimental determination of reaction kinetics and implications of the observed reaction rates for petroleum reservoirs. *Org. Geochem.* **35**, 393–404.

Davis J. B., Stanley J. P. and Custard H. C. (1970) Evidence against oxidation of hydrogen sulfide by sulfate ions to produce elemental sulfur in salt domes. *Am. Assoc. Petrol. Geol. Bull.* **54**, 2444–2447.

Ding K. L., Li S. Y., Yue C. T. and Zhong N. N. (2008) Simulation experiments on the reaction system of CH_4–$MgSO_4$–H_2O. *Chin. Sci. Bull.* **53**, 1071–1078.

Douglas A. G. and Mair B. J. (1965) Sulfur: role in genesis of petroleum. *Science* **147**, 499–501.

Dinur D., Spiro B. and Aizenshtat Z. (1980) The distribution and isotopic composition of sulfur in organic-rich sedimentary rocks. *Chem. Geol.* **31**, 37–51.

Feely H. W. and Kulp J. L. (1957) Origin of Gulf Coast salt dome sulfur deposits. *Am. Assoc. Petrol. Geol. Bull.* **41**, 1802–1853.

Garven G., Raffensperger J. P., Dumoulin J. A., Bradley D. A., Toung L. E., Kelley K. D. and Leach D. L. (2003) Coupled heat and fluid flow modeling of the carboniferous Kuna basin, Alaska: implications for the genesis of the Red Dog Pb–Zn–Ag–Ba ore district. *J. Geochem. Explor.* **78–79**, 215–219.

Goldhaber M. B. and Orr W. L. (1995) Kinetic controls on thermochemical sulfate reduction as a source of sedimentary H2S. In *Geochemical Transformations of Sedimentary Sulfur* (eds. M. A. Vairavamurthy, M.A.A. Schoonen). American Chemical Society Symposium Series 612. American Chemical Society, pp. 412–425.

Hao F., Guo T. L., Zhu Y. M., Cai X. Y., Zou H. Y. and Li P. P. (2008) Evidence for multiple stages of oil cracking and thermochemical sulfate reduction in the Puguang gas field, Sichuan Basin, China. *Am. Assoc. Petrol. Geol. Bull.* **92**, 611–637.

Heydari E. (1997) The role of burial diagenesis in hydrocarbon destruction and H2S accumulation, Upper Jurassic Smackover Formation, Black Creek Field, Mississippi. *Am. Assoc. Petrol. Geol. Bull.* **81**, 26–45.

Heydari E. and Moore C. H. (1989) Burial diagenesis and thermochemical sulfate reduction, Smackover Formation, southeast Mississippi salt basin. *Geology* **17**, 1080–1084.

Kiyosu Y. and Krouse H. R. (1993) Thermochemical reduction and sulfur behavior of sulfate by acetic acid in the presence of native sulfur. *Geochem. J.* **27**, 49–57.

Krouse H. R., Viau C. A., Eliuk L. S., Ueda A. and Halas S. (1988) Chemical and isotopic evidence of thermochemical sulfate reduction by light hydrocarbon gases in deep carbonate reservoirs. *Nature* **333**, 415–419.

Lu W. J., Chou I. M., Rurruss R. C. and Song Y. C. (2007) A unified equation for calculating methane vapor pressures in the CH_4–H_2O system with measured Raman shifts. *Geochim. Cosmochim. Acta* **71**, 3969–3978.

Machel H. G. (1987) Saddle dolomite as a by-product of chemical compaction and thermochemical sulfate reduction. *Geology* **15**, 936–940.

Machel H. G. (1989) Relationships between sulphate reduction and oxidation of organic compounds to carbonate diagenesis, hydrocarbon accumulations, salt domes, and metal sulphide deposits. *Carbonates Evaporites* **4**, 137–151.

Machel H. G. (2001) Bacterial and thermochemical sulfate reduction in diagenetic settings—old and new insights. *Sedim. Geol.* **40**, 143–175.

Machel H. G., Krouse H. R. and Sassen R. (1995) Products and distinguishing criteria of bacterial and thermochemical sulfate reduction. *Appl. Geochem.* **10**, 373–389.

Mankiewicz P. J., Pottorf R. J., Kozar M. G. and Vrolijk P. (2009) Gas geochemistry of the Mobile Bay Jurassic Norphlet Formation: thermal controls and implications for reservoir connectivity. *Am. Assoc. Petrol. Geol. Bull.* **93**, 1319–1346.

Mougin P., Lamoureux-Var V., Bariteau A. and Huc A. Y. (2007) Thermodynamic of thermochemical sulphate reduction. *J. Pet. Sci. Eng.* **58**, 413–427.

Orr W. L. (1974) Changes in sulfur content and isotopic ratios of sulfur during petroleum maturation—study of Big Horn Basin Palezoic oils. *Am. Assoc. Petrol. Geol. Bull.* **58**, 2295–2318.

Orr W. L. (1977) Geologic and geochemical controls on the distribution of hydrogen sulfide in natural gas. In *Advances in Organic Geochemistry* (eds. R. Campos and J. Goni). Enadisma, Madrid, Span, pp. 571–597.

Orr W. L. (1982) Rate and mechanism of non-microbial sulfate reduction. *Geol. Soc. Am. Abs. Prog.* **14**, 580.

Pan C. C., Yu L. P., Liu J. Z. and Fu J. M. (2006) Chemical and carbon isotopic fractionations of gaseous hydrocarbons during abiogenic oxidation. *Earth Planet. Sci. Lett.* **246**, 70–89.

Powell T. G. and Macqueen R. W. (1984) Precipitation of sulfide ores and organic-matter–sulfate reactions at Pin Oiont, Canada. *Science* **224**, 63–66.

Robinson B. W. (1973) Sulphur isotope equilibrium during sulphur hydrolysis at high temperatures. *Earth Planet. Sci. Lett.* **18**, 443–450.

Rhodes J. A. (1994) Reservoir property changes caused by thermochemical sulfate reduction in the smackover formation. *Gulf Coast Assoc. Geol. Soc. Trans.* **44**, 605–610.

Sangster D. F., Savard M. M. and Kontak D. J. (1998) A genetic model for mineralization of Lower Windsor (Visean) carbonate rocks of Nova Scotia, Canada. *Econ. Geol.* **93**, 932–952.

Sassen R. and Moore C. H. (1988) Framework of hydrocarbon generation and destruction in Eastern Smackover Trend. *Am. Assoc. Petrol. Geol. Bull.* **72**, 649–663.

Seewald J. S. (2003) Organic–inorganic interactions in petroleum-producing sedimentary basins. *Nature* **426**, 327–333.

Shang L. B., Chou I. M., Lu W. J., Burruss R. C. and Zhang Y. X. (2009) Determination of diffusion coefficients of hydrogen in fused silica between 296 and 523 K by Raman spectroscopy and application of fused silica capillaries in studying redox reactions. *Geochim. Cosmochim. Acta* **73**, 5435–5443.

Shang L. B., Chou I. M., Lu W. J. and Burruss R. C. (2008) Determination of diffusion coefficients of hydrogen in fused silica between 23 and 250 °C by Raman spectroscopy. *Am. Geophys. Union Abstr.*, MR33A–1839.

Sun Y. Z. and Puttmann W. (2000) The role of organic matter during copper enrichment in Kupferchiefer from the Sangerhausen basin, Germany. *Org. Geochem.* **31**, 1143–1161.

Thom J. and Anderson G. M. (2008) The role of thermochemical sulfate reduction in the origin of Mississippi Valley-type deposits. I. Experimental results. *Geofluids* **8**, 16–26.

Trudinger P. A., Chambers L. A. and Smith J. W. (1985) Low-temperature sulfate reduction: biological versur abiological. *Can. J. Earth Sci.* **22**, 1910–1918.

Truche L., Berger G., Destrigneville C., Pages A., Guillaume D., Giffaut E. and Jacquot E. (2009) Experimental reduction of aqueous sulphate by hydrogen under hydrothermal conditions: implication for the nuclear waste storage. *Geochim. Cosmochim. Acta* **73**, 4824–4835.

Toland W. G. (1960) Oxidation of organic compounds with aqueous sulphate. *J. Am. Chem. Soc.* **82**, 1911–1916.

Watanabe Y., Farquhar J. and Ohmoto H. (2009) Anomalous fractionations of sulfur isotopes during thermochemical sulfate reduction. *Science* **324**, 370–373.

Worden R. H. and Smalley P. C. (1996) H$_2$S-producing reactions in deep carbonate gas reservoirs: Khuff formation, Abu Dhabi. *Chem. Geol.* **133**, 157–171.

Worden R. H. and Smalley P. C. (2004) Does methane react during thermochemical sulphate reduction? Proof from the Khuff Formation, Abu Dhabi. In *Water–Rock Interaction 2004* (eds. R. Wanty and R. R. Seal). Taylor and Francis Group, London, pp. 1049–1053.

Worden R. H., Smalley P. C. and Oxtoby N. H. (1995) Gas souring by thermochemical sulfate reduction at 140 °C. *Am. Assoc. Petrol. Geol. Bull.* **79**, 854–863.

Worden R. H., Smalley P. C. and Oxtoby N. H. (1996) The effects of the thermochemical sulfate reduction upon formation water salinity and oxygen isotopes in carbonate gas reservoirs. *Geochim. Cosmochim. Acta* **60**, 3925–3931.

Worden R. H., Smalley P. C. and Cross M. M. (2000) The influence of rock fabric and mineralogy on thermochemical sulfate reduction: Khuff Formation, Abu Dhabi. *J. Sediment. Res.* **70**, 1210–1221.

Yuan S. D., Chou I. M., Li J. K. and Rurruss R. C. (2009) In-situ Raman spectroscopic Investigation of sulfur, sulfur–water, and sulfur–methane–water systems between 22 and 450 °C. *Am. Geophys. Union Abstr.*, V43B–2247.

Yue C. T., Li S. Y., Ding K. L. and Zhong N. N. (2005) Study of simulation experiments on the TSR system and its effect on the natural gas destruction. *Sci. China (Ser. D)* **48**, 1197–1202.

Yue C. T., Li S. Y., Ding K. L. and Zhong N. N. (2006) Thermodynamics and kinetics of reactions between C$_1$–C$_3$ hydrocarbons and calcium sulfate in deep carbonate reservoirs. *Geochem. J.* **40**, 87–94.

Zhang T. W., Amrani A., Ellis G. S., Ma Q. S. and Tang Y. C. (2008a) Experimental investigation on thermochemical sulfate reduction by H$_2$S initiation. *Geochim. Cosmochim. Acta* **72**, 3518–3530.

Zhang T. W., Ellis G. S., Walters C. C., Kelemen S. R., Wang K. S. and Tang Y. C. (2008b) Geochemical signatures of thermochemical sulfate reduction in controlled hydrous pyrolysis experiments. *Org. Geochem.* **39**, 308–328.

Associate editor: Jeffrey C. Alt